SS-157
2121

A MULTIPARTICLE SPECTROMETER DESIGN FOR NAL

A. W. Key

J. A. Matthews

P. M. Patel

J. D. Prentice

J. Vavra

and

T-S Yoon

Experiments Design Program, McGill University

ABSTRACT

This paper presents the design of a multiparticle spectrometer useful for the on-line accumulation of data on a variety of high-energy reactions at NAL. In order to be specific, the spectrometer has been designed to provide complete momentum and angular coverage for the products of the reaction $\pi p \rightarrow p3\pi$ at 100 GeV/c, with accuracies $\delta p \simeq 0.1$ GeV/c and $p\delta\theta \lesssim 0.02$ GeV/c. The detectors are assumed to be wire planes with a spatial resolution of 0.2 mm, internal or external to a magnetic field. The momentum analyzer consists of a magnetic field of 20 kG over a volume $8 \times 1.6 \times 0.8$ m^3, followed by a downstream lever arm of length 16 m. Beam requirements, detection of neutrals, and triggering criteria for the specific reaction considered, are briefly discussed. Two appendices give formulae for the calculation of measurement errors inherent in this type of system and an indication of the saving in magnet size resulting from a relaxation of the accuracy requirements.

INTRODUCTION

In March 1969 the Canadian 200-GeV Study Group proposed to the National Research Council of Canada that there be direct Canadian participation in NAL. As part of this effort NAL invited several Canadian physicists to participate in the 1969 Summer Study at Aspen. These physicists provided links between the Summer Study and an Experiments Design Program which the 200-GeV Study Group organized at McGill University in

Montreal from July 6 to 18. The participants in this program were particle physicists from across Canada who were interested in learning about and designing experiments for NAL. They produced a series of papers relating to the theoretical and experimental problems of physics at NAL energies. The majority of the experimental papers concentrated on topics relating to the design of a spectrometer capable of studying a variety of high-energy reactions. Additional details were worked out at Aspen and at Montreal, and the proceedings of the Experiments Design Program have now been edited into one large report.

Since this work is closely connected to that of the 1969 Summer Study, it was felt worthwhile to produce a self-contained report summarizing the content of a selection of these papers for inclusion in the present volume.

I. PREAMBLE

The increasing particle multiplicity at high energies makes it inevitable that a multiparticle spectrometer will prove to be a very useful and versatile instrument at NAL. At presently existing energies a substantial fraction of the secondaries from inelastic collisions are emitted with low energies at large laboratory angles. An extrapolation of these results to higher energies indicates that a multiparticle spectrometer for NAL must cover a large solid angle.

We list some of the experiments which could be effectively performed with such a spectrometer:

1. Diffractive and peripheral production of hadron resonances of mass $\lesssim 3$ GeV/c^2, using hydrogen and deuterium as targets. The limitation on mass is imposed by the demand for very high efficiency in angular and momentum acceptance for the detection of the reaction products. This demand is dictated by the belief that a knowledge of the density matrix elements which are deduced from the angular distribution of the decay products is not only essential for determining the spin and parity of the resonance but is also vital for the elucidation of the production mechanism. In counter and spark-chamber experiments at existing energies, this provision of high efficiency has been traditionally treated as a luxury to be relegated to second generation experiments. We feel strongly that this should not be the case at NAL.

2. Diffractive production of hadron resonances of mass $\lesssim 3$ GeV/c^2, using complex nuclei as targets. The object here is to measure the unstable particle-nucleon cross sections and to learn whether a proposed resonance is really a resonance or a kinematic enhancement. In addition, the presence of strong coherence in particle production on a nucleus would be a direct verification of the diffractive nature of the corresponding particle-nucleon reaction. The attractiveness of high-energy physics with complex nuclei has been emphasized by B. Margolis and collaborators.[1]

3. Peripheral production of hadron resonances of mass $\gtrsim 3$ GeV/c^2. The decay products are detected with partial efficiency. The object here would be to study the resonance spectrum. As Walker[2] has emphasized, the traditional missing mass survey experiments, where one studies the angle and/or momentum of the recoil proton only, will be extremely difficult at NAL energies because present-day techniques make it hard to achieve the accuracy necessary in measuring the longitudinal component of the low-momentum recoil proton to attain good resolution in the mass of the resonance. These arguments do not rule out, however, the use of the effective mass technique in survey experiments where the relatively inaccurate recoil proton information supplements accurate measurement on the decay products even though one might not have full efficiency for detecting the latter.

4. Strange particle studies. We expect that the NAL 200-GeV primary beam interacting with complex targets (Be or Cu) will give secondary beams of K mesons, of energy 20 GeV and up, which are an order of magnitude higher in intensity than presently available beams. It will thus be possible to mount strange hadron physics experiments such as spectrum survey and production mechanism studies which are not presently possible. The spectrometer proposed here could be modified to include rather modest Cerenkov counters to distinguish between pions and kaons.

II. REACTION

We have taken a specific reaction--diffractive and peripheral production of 3π's in π-p collisions at 100 GeV--in order to get a fairly good idea of the size of the device. To calculate the kinematics we have assumed that the decay chain proceeds as follows

$$\begin{array}{l} \pi^- + p \rightarrow X^- + p \\ \qquad\quad \lfloor\!\rightarrow \rho^0 + \pi_1^- \\ \qquad\qquad \lfloor\!\rightarrow \pi_2^+ + \pi_3^- . \end{array}$$

For simplification, we assume that the production and decay occur in the same plane. While this is clearly a special case and may be grossly inaccurate for calculating the efficiency of the system, it is reliable for estimating the momentum range to be expected and the maximum laboratory angles at which pions of given momenta occur. In a detailed calculation, these restrictions and also that of the $\rho\pi$ intermediate state would be eliminated.

We impose the following restrictions on the design:

1. The design must call for a minimum amount of hardware innovation. This, for instance, restricts us to at most 20-kG fields in our large aperture magnet.

However, in the use of wire spark chambers we have not been inhibited from demanding designs to be used in a magnetic field with spatial resolution of up to 0.20 mm. The development in wire chambers of different types is so rapid that we expect these criteria will be met; in addition, chambers run in the proportional mode may be incorporated as part of the trigger logic. Of course, for chambers external to the magnetic field, standard magnetostrictive readout planes are adequate.

2. The device must be fully capable of on-line data processing. This for instance, eliminates the use of optical spark chambers and streamer chambers when we impose restriction (1) at the same time.

3. The device must have a high efficiency in angular and momentum acceptance for detecting and measuring the decay products of X when the mass of X is restricted to be $\lesssim 3$ GeV/c^2. The arguments for this have been given in the preamble.

4. The device should detect the recoil proton where this is kinematically possible.

5. The design should incorporate high-efficiency γ-ray shower chambers and counters to deduce the neutral pion emission angle and energy from measurements on the photon shower production and development. The detailed design of these detectors, the calculation and provision of the required accuracy in measuring angle and energy of the showers, and the accurate evaluation of their efficiency is non-trivial. The wire-chamber assemblies and the lead-scintillator sandwiches or lead-glass counters will involve considerable expense. However, as Walker[2] has emphasized, neutral particle detection is essential for any multiparticle spectrometer design. These counters will cover the interior of the magnet aperture and additional counters will be placed downstream.

6. The level of efficiency attainable in the neutral detectors has a strong bearing on the measurement accuracy necessary. If the π^0's can be detected with very high efficiency over the entire solid angle, events with no, one, and many π^0's can be easily separated from each other. However, if the detection efficiency for the π^0's is appreciably less than 100%, adequate separation of the different event types must rely on the kinematics, and the necessary measurement accuracy must be greatly improved.

We have adopted the more pessimistic assumption in the present design since a full investigation of the cost and efficiency of π^0 detectors has not been made. The necessary momentum and angular accuracies in this case are

$$\delta p \simeq 0.1 \text{ GeV/c}; \quad p\delta\theta \simeq 0.02 \text{ GeV/c}.$$

Since our arguments for these numbers are basically those presented in the 1968 NAL Summer Study,[3] they will not be given here.

Since it is of interest to know the effects of the assumption that all neutral pions can be detected with full efficiency, we have investigated this question in some detail. Our results are given in Appendix II.

III. RESTRICTIONS ON THE RANGE OF 4-MOMENTUM TRANSFER t

From the Rapporteur's talk by Bellettini[4] at Vienna, it is clear that for diffractive processes the range of t explored must include $t \approx 1\ (\mathrm{GeV/c})^2$, where a break in the slope of $d\sigma/dt$ occurs. Initially, from $t = t_{min}$ to $t = 1\ (\mathrm{GeV/c})^2$, the cross section behaves as

$$\frac{d\sigma}{dt} = Ae^{-bt},$$

where $b \approx 7.5\ (\mathrm{GeV/c})^{-2}$. The fall-off thereafter is much flatter and varies from reaction to reaction.

In most theoretical models, the diffractive cross section has, at most, a very weak logarithmic energy dependence and therefore, from the knowledge of the cross section at presently accessible energies ($\approx 180\ \mu b$ at 25 GeV/c) and the typical beam intensities expected at NAL, we conclude that we shall not be plagued by vanishing event rates. We have designed the spectrometer aperture to cover the range $(t - t_{min}) \approx 1\ (\mathrm{GeV/c})^2$, so that given the above value of the slope b, we shall be accepting almost the full diffractive cross section in our apparatus.

IV. KINEMATICS

A simple kinematics program generated Figs. 1 to 5, from which the following information is extracted concerning the maximum apertures necessary:

p_{inc} = 100 GeV/c
M_x = 1 to 3 $\mathrm{GeV/c}^2$
$t_{max} = 1.1\ (\mathrm{GeV/c})^2$

Protons

θ_p (minimum) = 58°
θ_p (maximum) = 85°
p_p (maximum) = 1.2 GeV/c
p_p (minimum) = 0.2 GeV/c (minimum momentum for which protons will emerge from the target).

Pions

$$\theta(\pi_1)^{(max)} = 17^\circ \rightarrow p(\pi_1) = 0.5 \text{ GeV/c}$$

$$\theta(\pi_2)^{(max)} = \theta(\pi_3)^{(max)} = 13.4^\circ \rightarrow p_\pi = 0.66 \text{ GeV/c}$$

$$p(\pi) = 50 \text{ GeV/c} \rightarrow \theta(\pi_1)^{(max)} = 2.5^\circ$$

$$\rightarrow \theta(\pi_2)^{(max)} = 2.5^\circ .$$

$$p(\pi) = 15 \text{ GeV/c} \rightarrow \theta(\pi_1)^{(max)} = 3.8^\circ$$

$$\rightarrow \theta(\pi_2)^{(max)} = 3.8^\circ$$

$$\theta(\pi)^{(min)} \approx 0^\circ \rightarrow p(\pi)^{(max)} \approx 100 \text{ GeV/c}.$$

It is interesting to note that, in the model assumed, where ρ mediates the X decay:

$$X \rightarrow \rho + \pi_1$$

$$\rightarrow \pi_2 + \pi_3 ,$$

the parameters of π_1 determine the aperture of the spectrometer.

V. BEAM AND TARGET

In deciding on the beam characteristics and target size required for this experiment we have drawn heavily on the draft copy of the 1969 Summer Study report by Reeder.[5] The most suitable beam is the 2.5 mrad unseparated beam from target-station 2. Tune 1 of this beam gives 6.9×10^5 π^- per pulse at 100 GeV/c, with a momentum bite of 0.5%. This implies that at the 0.1% momentum resolution necessary for this experiment, the intensity will be 1.4×10^5 π^- per pulse. If it becomes necessary to improve this resolution even further, the beam momentum can be measured by a hodoscope at the momentum dispersed horizontal focus.

With a trigger consisting of 3 or 4 charged particles emitted from the target (depending on the t range being studied) and no neutrals, we estimate a signal to background ratio of about 1:10. If it is assumed that the diffractive dissociation cross section is about 150 μb at 100 GeV/c, a beam intensity of 1.4×10^5 π^- per pulse together with a 10-cm long liquid hydrogen target is sufficient to saturate the expected data-handling rate of 10 msec per event. This will give about 5-10 good events per pulse.

The beam size at the final focus of the 2.5 mrad beam is 0.9×0.75 mm^2. We thus envisage a target with a diameter of about 2 mm to accommodate this beam.

The uncertainty in the transverse beam momentum caused by the beam divergence is about 0.08 GeV/c. To maintain the required accuracy of $p\delta\theta \simeq 0.02$ GeV/c, it will thus be necessary to use a proportional wire chamber placed at the exit to the last quadrupole to measure the beam divergence. A plane of 8 cm diameter which provides 40 bins will reduce the $p\delta\theta$ of the beam to a negligible level.

VI. SPECTROMETER DESIGN

A. Recoil Protons

As discussed in the previous section the target radius will be typically 1 mm. Hence, protons of momentum greater than 200 MeV/c will easily escape from the target assembly. This corresponds to $t \simeq 0.04$ (GeV/c)^2. We therefore conceive of the measurements being done in two stages:

1. $t_{min} < t < 0.04$ (GeV/c)^2: The proton does not leave the target.
2. 0.04 (GeV/c)$^2 < t < 0.2$ (GeV/c)^2: The proton leaves the target, but is still very slow and therefore its energy is conveniently obtained by range measurements.

These two ranges of t can be covered by the same target-associated setup, ahead of the spectrometer magnet, as shown in Fig. 6. As discussed in the preamble, we do not intend to use the measurements on the protons to determine the missing mass with good resolution. In conjunction with the measurements on the neutral and charged pions, the proton parameters pin down the reaction and help in the effective mass determination.

The target is surrounded by an array of wire spark-chamber planes. The first two planes (A and B) are separated sufficiently to give an angular resolution of approximately 5 mrad. TSC1 is a thin scintillation counter which is used for pulse height analysis. C, D, etc., are wire planes interleaved with thin absorbers to measure the energy to approximately 5 MeV. The scintillation counter TSC2 is used in anticoincidence to indicate that no charged particle of momentum $\gtrsim 500$ MeV/c passed through the target assembly. For the lowest t values and for diffraction production experiments on complex nuclei, TSC1 will be used in anticoincidence. Figure 6 also shows a possible neutral detection configuration.

3. 0.2 (GeV/c)$^2 < t < 1.1$ (GeV/c)^2: The magnetic analysis of the proton momentum becomes quite convenient and the best way to achieve this is to move the target into the magnet as shown in Fig. 7. The thin scintillation counter jacket around the target signifies a charged particle emitted by the target at angles greater than about 20°. It is true that for events with higher multiplicity than 3, there may be

charged pions emitted at angles greater than 20°. However, a post event kinematic fit can easily eliminate these.

B. Pions

The pions have a momentum range of $0.5 < p < 100$ GeV/c, and an angular range of $0 < \theta \leq 18°$.

It may be of interest to trace the evolution of the final design we present in a preliminary version below. The unsuccessful candidates were:

1. Target with wire-chamber assembly in a magnet M-1 to measure pions of momenta less than 3 GeV/c. A magnet M-2 with external wire chambers to span the momentum range $3 < p < 100$ GeV/c.

2. M-1 same as in (1), but M-2 replaced by two magnets M-2' and M-2" to span the momentum ranges $3 < p < 20$ GeV/c and $20 < p < 100$ GeV/c. A factor of two reduction in the effective magnetic volume necessary is thus achieved.

3. M-1 and M-2 combined to span the range $0.5 < p < 25$ GeV/c. A separate magnet with symmetrical input and output spark chambers handled the momentum range $25 < p < 100$ GeV/c.

4. All the magnets combined into one, which is filled with wire spark chambers to cover the full momentum and angular range given above. This is cheaper than design (3), even though the magnet is extremely large.

Downstream Lever Arm

It has been noted[6] by L. Osborne, W. Selove, and others (see, e.g., SS-86) that in magnets of the CERN Omega type, the accuracy in the momentum measurement of the pions which leave the magnet can be considerably improved by providing external spark chambers to get a long lever arm downstream. In particular, the size of the magnet in case (4) can be almost halved. We have assumed in the design that each wire spark assembly, consisting of six planes, provides a measurement of the x-coordinate, y-coordinate, and ω (diagonal) coordinates, and that the spatial resolution is ± 0.20 mm. The effective thickness per chamber of 2×10^{-3} radiation lengths that we have assumed is conservative and can be considerably increased without affecting the design. The magnetic field is set at 20 kG although the choice between a cryogenic, a superconducting, or a conventional magnet is left open.

Figures 8 and 9 give a sketch of the system we envisage. Appendix I lists the formulae used for calculations of the momentum and angular resolution and discusses the salient points. We have not attempted a systematic optimization of the various parameters. At this preliminary stage, it seemed appropriate to take various configurations and feed them into a short programme which calculated the measuring and

multiple scattering errors expected. We then chose the best configuration. The resultant parameters are summarized in Table I. The accuracy in the momentum and angle determinations for various momenta is shown in Figs. 11 and 12.

The length of the magnet is determined by the accuracy with which one wants to measure the highest momentum, using the spark chambers internal and external to the magnet. This length, together with the distribution of spark chambers in the magnet, determines the highest momentum one can measure without using the external lever arm. This in turn determines the vertical aperture by the requirement that all pions of momentum greater than this maximum limit be allowed to escape the magnet. It is the dispersion of the highest momentum measured internally that determines the horizontal aperture. The calculated dimensions listed in Table I will have to be increased to allow space for the trigger and shower counters.

Table I. Multiparticle Spectrometer Parameters.

Highest pion momentum measured internally	20 GeV/c
Length of Magnet (M)	8 m
Width of Magnet (W)	1.6 m
Gap of Magnet (H)	0.8 m
Magnet field (B)	20 kG
External Lever Arm (L)	16 m
Spatial resolution of spark planes (δy)	0.2 mm
Width of downstream spark planes (W_{ext})	6.5 m
Height of downstream spark planes (H_{ext})	2.5 m
No. of planes round target (n_1)	4
No. of planes at magnet exit (n_2)	4
No. of planes downstream (n_3)	2
No. of planes in magnet (N)	16

VII. FURTHER WORK

This is a preliminary design study. It must be followed up with detailed Monte Carlo studies to confirm the apertures and the accuracy claimed above. In addition, the design of a proper trigger system for a particular reaction is crucial. As mentioned previously, the provision of a neutral detection system is a necessity and is going to be expensive. The shower detectors will necessitate a substantial amount of development and experimental work.

Some preliminary thoughts on these problems, along with initial cost estimates of the spectrometer, are given in the Proceedings of the Experiments Design Program.[7]

APPENDIX I. ERROR CALCULATIONS

Notation:
- p = laboratory momentum of particles (GeV/c)
- θ = laboratory production angle of particle (radians)
- α = angle of bend in magnetic field (radians)
- B = field (kG)
- R = radius of curvature (m)
- W = width (horizontal) of magnet (m)
- M = length of magnet (m)
- H = height of magnet (m)
- ℓ_{int} = length of particle path in field (m)
- L_1 = projection of ℓ_{int} in beam direction (m)
- δy = positional accuracy of wire planes (m)
- L = length of lever arm (m)
- n_1 = number of planes round target
- n_2 = number of planes immediately after magnet
- n_3 = number of planes immediately after lever arm
- N = number of planes distributed uniformly through magnetic volume (in addition to n_1)
- t = thickness of one plane in radiation lengths
- ℓ_T = length of liquid H_2 traverse by particle (cm)
- X_0 = radiation length of liquid H_2 (cm)

Refer to Fig. 10 for a sketch of angles and dimensions listed above.

A. One Magnet, Two Equal Lever Arms

The error in measuring momentum in a magnet with two external lever arms [see Fig 10(a)] is given by

$$\frac{\delta p}{p} = \frac{p\delta\alpha}{0.03\ BM}, \tag{1}$$

neglecting multiple scattering.

Now

$$\delta\alpha = \frac{2\delta y}{L}. \tag{2}$$

Thus

$$\frac{\delta p}{p} = \frac{2p\delta y}{0.03\ BML}. \tag{3}$$

B. One Magnet, One Lever Arm

For a given momentum p, at a given production angle θ, the radius of curvature is given by

$$R = \frac{p}{0.03\ B} . \tag{4}$$

To find α, the angle of bend in a magnet of given width W, the relation is

$$\sin \alpha/2 = \frac{W}{4R \sin(\theta + \alpha/2)} , \tag{5}$$

which may be solved for α by interation. In the present calculation, the nth iteration is accepted when it differs by less than 1% from the (n-1)th iteration. [See Fig. 10(b), (c), and (d)].

To find α for a particle which leaves a magnet of length M before striking the side, the relation is

$$\sin \alpha/2 = \frac{M}{2R \cos(\theta + \alpha/2)} . \tag{6}$$

If then the minimum of the solutions of (5) and (6) is taken, the length of the particle path in the magnet is given by

$$\ell_{int} = \frac{p\alpha}{0.03\ B} . \tag{7}$$

The projection of this length in the beam direction is given by

$$L_1 = 2R \sin\left(\frac{\alpha}{2}\right) \cos\left(\theta + \frac{\alpha}{2}\right) . \tag{8}$$

Gluckstern[8] has given formulae for the accuracy with which p and θ can be measured in a magnet which has n coordinate measurements uniformly spaced along the particle path. He obtains

$$\left(\frac{\delta p}{p}\right)^{meas}_{int} = \frac{p\ \delta y}{0.03\ B \ell^2_{int}} \left(A_n\right)^{1/2} , \tag{9}$$

and

$$(\delta\theta)_{int}^{meas} = \frac{\delta y}{\ell_{int}} \left(B_n\right)^{1/2}, \tag{10}$$

where A_n and B_n are constants given by

$$A_n = \frac{720\, n^3}{(n-1)(n+1)(n+2)(n+3)}; \quad B_n = \frac{12(2n+1)(8n-3)n}{(n-1)(n+1)(n+2)(n+3)}. \tag{11}$$

Here it is assumed that

$$n = n_1 + NL_1/M. \tag{12}$$

The contribution to the errors caused by multiple scattering in the planes is given by

$$\left(\frac{\delta p}{p}\right)_{int}^{coul} = \frac{0.015}{0.03\, B\ell_{int}} \left[(n-1)t\right]^{1/2}, \tag{13}$$

and

$$(\delta\theta)_{int}^{coul} = \frac{0.015}{p} \left[(n-1)t\right]^{1/2}. \tag{14}$$

Multiple scattering in the target contributes to the error in angle only: it is represented by

$$(\delta\theta)^{target} = \frac{0.015}{p} \left(\ell_T/X_0\right)^{1/2}, \tag{15}$$

ℓ_T, the length of target traversed by the particle was approximated by

$$\ell_T = \text{minimum of } \left\{\left[\left(\frac{5}{0.1/\tan\theta}\right)\right]\right\} \text{ cm}. \tag{16}$$

The contribution to the momentum and angle errors for particles measured using the downstream lever arm and the chambers round the target are given by

$$\left(\frac{\delta p}{p}\right)_{ext}^{meas} = \frac{2p\,\delta y}{0.03\, BM^2} \left[\frac{1}{n_1} + \frac{1}{n_2}\left(1 + \frac{M}{L}\right)^2 + \frac{1}{n_3}\left(\frac{M}{L}\right)^2\right]^{1/2} \tag{17}$$

$$\left(\frac{\delta p}{p}\right)_{ext}^{coul} = \frac{0.015}{0.03\ BM}\left[\left(n_1 + n_2 + n_3 + N - 1\right)t\right]^{1/2}, \tag{18}$$

$$(\delta\theta)_{ext}^{meas} = \frac{\delta y}{M}\left[\frac{4}{n_1} + \frac{1}{n_2} + \left(2 + \frac{M}{L}\right)^2 + \frac{1}{n_3}\left(\frac{M}{L}\right)^2\right]^{1/2}, \tag{19}$$

$$(\delta\theta)_{ext}^{coul} = \frac{0.015}{p}\left[\left(n_1 + n_2 + n_3 + N - 1\right)t\right]^{1/2}. \tag{20}$$

The horizontal dimension of the downstream chamber is given by

$$W_{ext} = W + 2L\tan(\theta + \alpha). \tag{21}$$

APPENDIX II

The object of this appendix is to study in some detail the contributions to the error in the measurement of the effective mass of the X meson produced in the reaction $\pi^- p \to pX^- \to p3\pi$, and to investigate the modifications to the design of the spectrometer presented in the text if it is demanded only that this mass be determined to 30 MeV/c^2. As discussed above, if it is necessary to measure pion momenta and angles with sufficient accuracy to distinguish events with missing neutrals on the basis of the kinematics alone, the required tolerances would be much more restrictive than those presented in this appendix.

The symbols used in the following error calculations are explained in Fig. 13. The invariant mass M_X of the 3π system can be expressed by:

$$M_X^2 = \left(E_1 + E_2 + E_3\right)^2 - \left(\vec{p}_1 + \vec{p}_2 + \vec{p}_3\right)^2.$$

We decompose $\vec{p}_i$ into parallel and longitudinal components ($\vec{p}_{\parallel i}$ and $\vec{p}_i$) and use the approximation

$$p_{\parallel i} = p_i \cos\theta_i \simeq p_i\left(1 - \frac{\theta_i^2}{2}\right).$$

Also we use the relativistic approximation

$$E_i = \left[p_i^2 + m_\pi^2\right]^{1/2} \simeq p_i + \frac{m_\pi^2}{2p_i}.$$

We get,

$$M_X^2 \simeq \left(p_1 + p_2 + p_3\right)\left[\left(\frac{1}{p_1} + \frac{1}{p_2} + \frac{1}{p_3}\right) m_\pi^2 + p_1\theta_1^2 + p_2\theta_2^2 + p_3\theta_3^2\right] - \left(\Sigma\vec{p}_{\perp i}\right)^2 .$$

The sum of the transverse components, $\Sigma\vec{p}_{\perp i}$, is equal to the transverse components of the recoiling proton, and therefore its contribution to M_X^2 is small in the low t region. Furthermore, if the recoil proton is measured, then, the additional constraints would make the error contribution from this term negligible. For these reasons, we consider only the expression

$$M_X^2 \simeq \Sigma p_i \left(m_\pi^2 \; \Sigma \frac{1}{p_i} + \Sigma p_i \theta_i^2\right) . \tag{1}$$

We can make the following simple observations:

1. To achieve a good mass resolution, we strive for

$$\delta\left(p_1\theta_1^2\right) \simeq \delta\left(p_2\theta_2^2\right) \simeq \delta\left(p_3\theta_3^2\right) .$$

This means that we need accurate momentum measurements on large angle tracks and accurate angle measurement on those tracks with large values of $p_i\theta_i$ (transverse momentum).

2. The presence of the $1/p_i$ term indicates that we need accurate measurement of momentum of low momentum tracks (~1 GeV/c).

3. Now,

$$\delta\left(p_i\theta_i^2\right) = \delta p_i \theta_i^2 + 2p_i\theta_i\,\delta\theta_i$$

$$= p_i\theta_i^2\left(\frac{\delta p_i}{p_i} + 2\,\frac{\delta\theta_i}{\theta_i}\right) .$$

This shows that the percent error of the momentum can be as large as the percent error on angle measurement.

To do some specific calculations we differentiate (1) to obtain

$$\delta\left(M_X^2\right) = 2M_X\,\delta M_X$$

$$= \sum_j \delta p_j \left(\frac{M_X^2}{p_0} + \theta_i^2 p^o - \frac{m^2}{p_j^2} p^o\right) + 2\sum_j \delta\theta_j p^o p_j \theta_j , \tag{2}$$

where we put

$$p^o \equiv p_1 + p_2 + p_3 \approx 100 \text{ GeV/c}.$$

The error in M_X has been calculated from (2) for a few representative examples of the decay $X \to 3\pi$, assuming that

$$\frac{\delta p_i}{p_i} = 0.5\%$$

and

$$\delta\theta_i = 0.5 \text{ mrad}.$$

The results are summarized in Table II. All quoted errors are rms errors. The results are consistent with the previous observations 1, 2, and 3. Examination of the table shows that 0.4 mrad in $\delta\theta$ and 0.5% in $\delta p/p$ is ample to give a δM (rms) of 30 MeV/c^2, as required.

Table II. Errors in Missing Mass Determination.

	δM_X for Five Typical Cases				
	Case (a)	(b)	(c)	(d)	(e)
M_X	3 GeV/c^2	3	3	3	1.2
p_1	33 GeV/c	80	90	10	80
p_2	33	10	5	45	10
p_3	33	10	5	45	10
θ_1	30×10^{-3} rad	0	0	0	10
θ_2	30	65	90	31	10
θ_3	30	65	90	31	10
Contribution to δM from δp_1	3 MeV/c^2	6	7	1	5
Contribution to δM from δp_2	3	3	3	7	1
Contribution to δM from δp_3	3	3	3	7	1
Contribution to δM from $\delta\theta_1$	17 MeV/c^2	0	0	0	33
Contribution to δM from $\delta\theta_2$	17	11	7.5	23	4
Contribution to δM from $\delta\theta_3$	17	11	7.5	23	4
δM_X combined	30 MeV/c^2	17	14	33	33

In designing the spectrometer, we actually took $(\delta p/p) = 0.5\%$ and $(p\delta\theta) = 0.01$ GeV/c. Assuming a spatial resolution of 0.25 mm, we obtain the parameters of Table III.

Table III. Alternative Spectrometer Parameters.

Highest pion momentum measured internally	15 GeV/c
Length of magnet (M)	4 m
Width of magnet (W)	1.5 m
Gap of magnet (H)	0.7 m
Magnetic field (B)	20 kG
External lever arm (L)	8 m
Width of downstream spark planes (W_{ext})	6 m
Height of downstream spark planes (H_{ext})	2 m
No. of planes round target (n_1)	2
No. of planes at magnet exit (n_2)	6
No. of planes downstream (n_3)	4
No. of planes in magnet (N)	5

A comparison with the design parameters given in Table I shows that the magnet length and the external lever arm have been halved, with a corresponding decrease in the number and size of the wire chambers necessary. A sketch of the design and the dependence of the momentum and angular resolution on the pion momentum appear in Figs. 14 to 16.

REFERENCES

[1] K. S. Koldig and B. Margolis, Nucl. Phys. B6, 85 (1968).

[2] W. D. Walker, On the Use of a Hybrid Bubble Chamber in the 100-BeV Region, National Accelerator Laboratory 1968 Summer Study Report A. 3-68-100, Vol. III, p. 299.

[3] T. Fields et al., A Hybrid Detector System for 100-GeV Strong Interactions, National Accelerator Laboratory 1968 Summer Study Report A. 3-68-12 (Revision), Vol. III, p. 227.

[4] G. Bellettini, Proceedings of the XIV International Conference on High Energy Physics, Vienna, 1968, p. 329.

[5] D. Reeder, High Quality Unseparated Beams, National Accelerator Laboratory 1969 Summer Study Report SS-41, Vol. I.

[6]L. S. Osborne, Design Criterion for Magnetic Spectrometers, National Accelerator Laboratory 1969 Summer Study Report SS-86, Vol. III; W. Selove et al., The Alpha Project, National Accelerator Laboratory 1969 Summer Study Report SS-86, Vol. III.

[7]Proceedings of the Canadian 200 GeV Experiments Design Programme, Montreal, July 1969, edited by P. M. Patel.

[8]R. Gluckstern, Nucl. Instr. and Methods 24, 381 (1963).

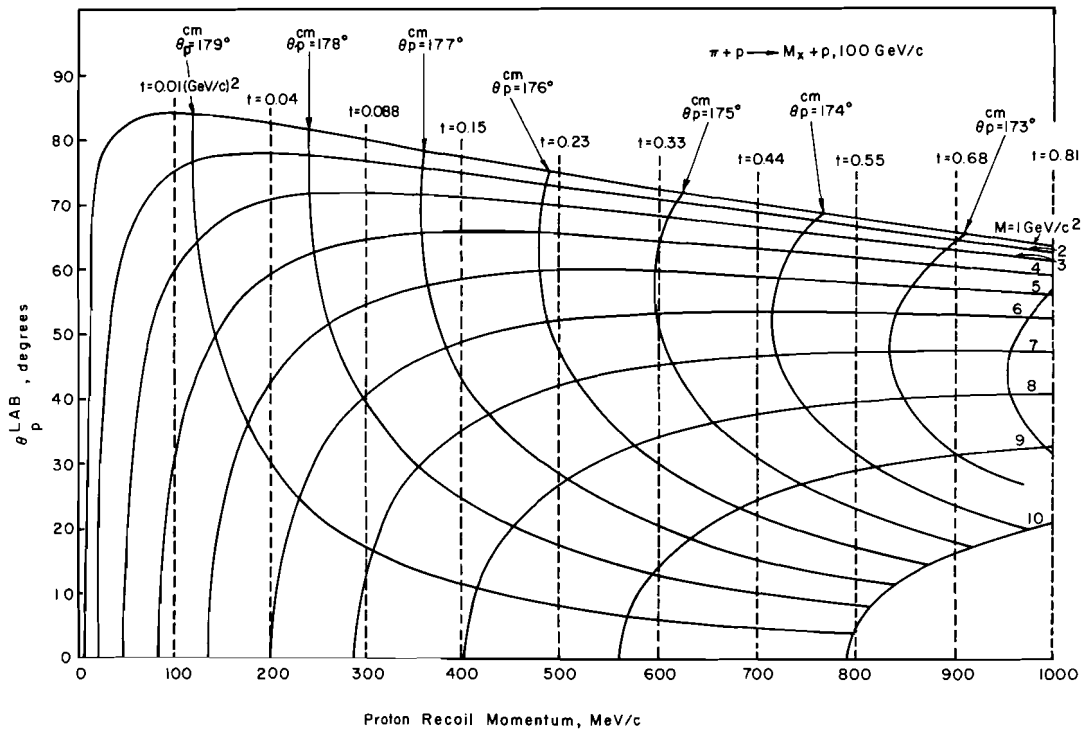

Fig. 1. Momentum vs angle of the proton produced in the reaction $\pi p \rightarrow xp$ at 100 GeV/c as a function of the mass M_x of X. Values of the squares of the four-momentum transfer (t) to the proton and proton production angle in the center-of-mass (θ_p^{cm}) are indicated.

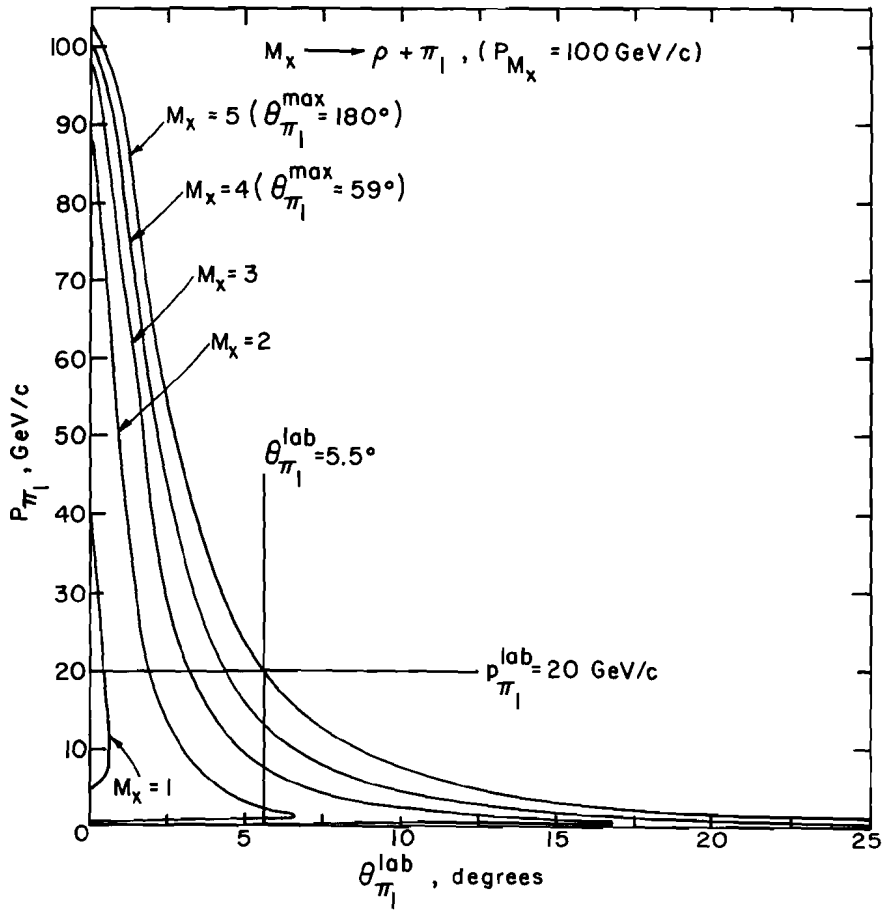

Fig. 2. Angle vs laboratory momentum of the pion produced in the decay $X \rightarrow \pi_1 \rho$ at 100 GeV/c, as a function of the mass M_x of X.

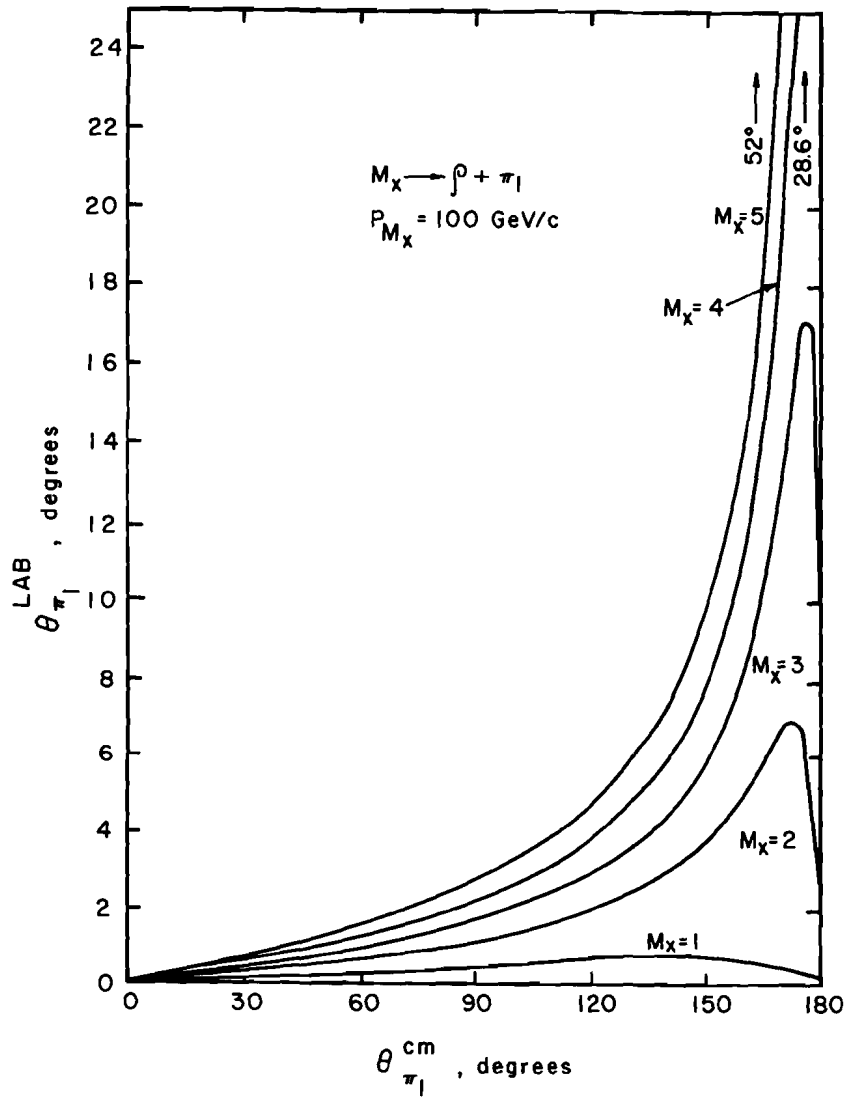

Fig. 3. Center-of-mass vs laboratory angle for the pion produced in the decay $X \rightarrow \pi_1 \rho$ at 100 GeV/c, as a function of the mass of X.

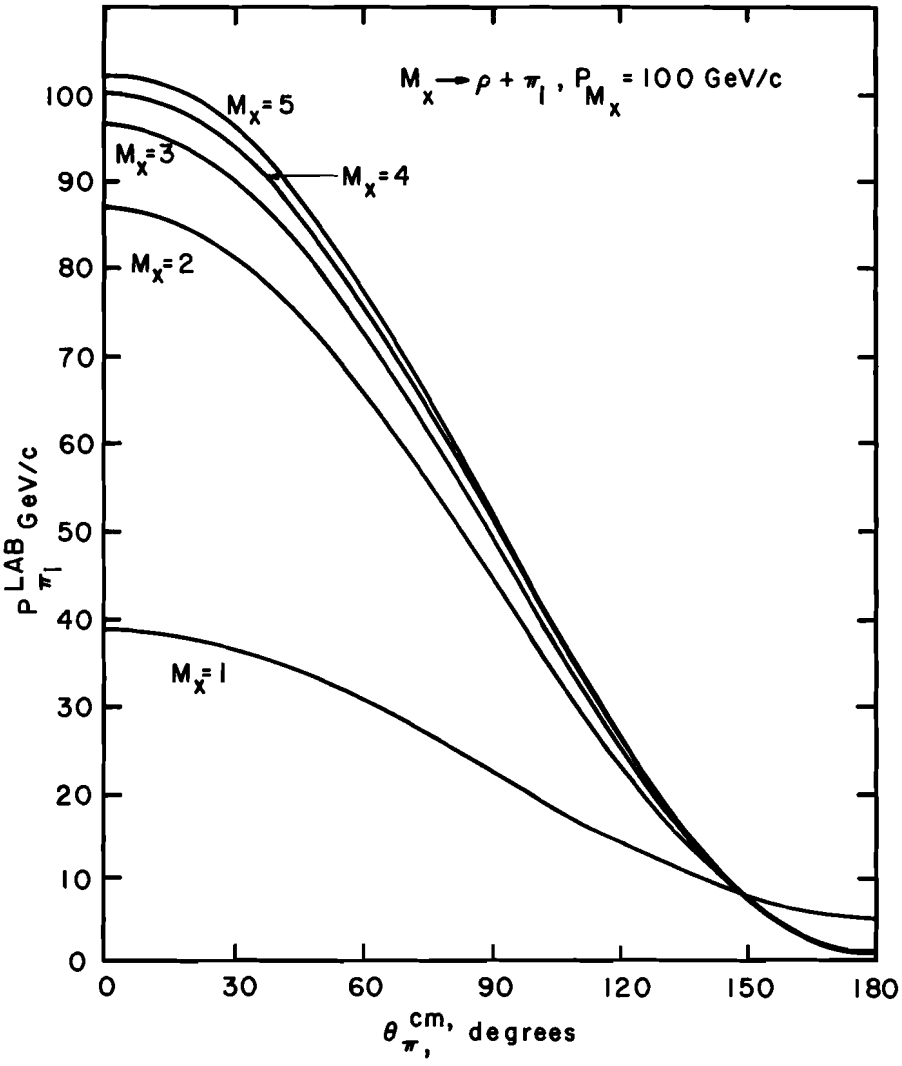

Fig. 4. Center-of-mass angle vs laboratory momentum of the pion produced in the decay $X \rightarrow \pi_1 \rho$ at 100 GeV/c, as a function of the mass of the X.

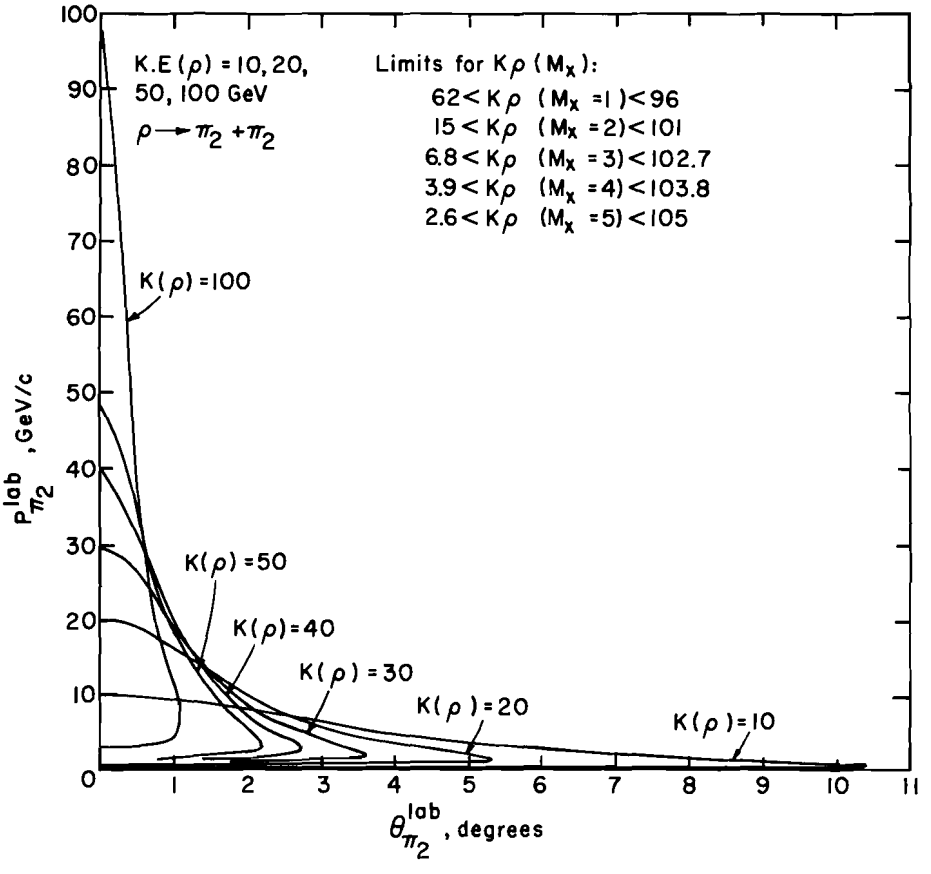

Fig. 5. Laboratory angle vs laboratory momentum of the pion from ρ decay, where the ρ is produced from the decay of a 100 GeV/c X meson: $X \rightarrow \pi_1 \rho \rightarrow \pi_1 \pi_2 \pi_2$. The curves are labeled by the kinetic energy in GeV of the ρ meson, K(ρ). The limits on the values of K(ρ) for different values of M_x are given.

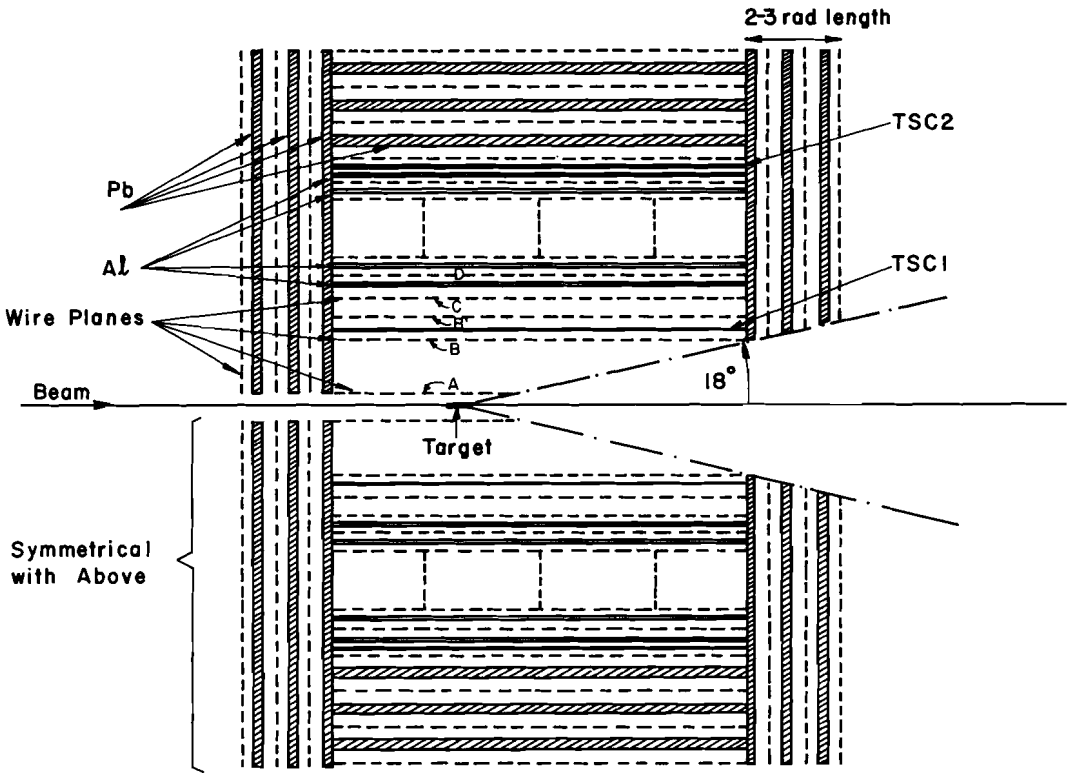

Fig. 6. System of neutral and charged-particle detectors surrounding a liquid hydrogen target for the study of the reaction $\pi p \rightarrow pX$ at 100 GeV/c, in the case when the proton does not leave the target. See text for a full description.

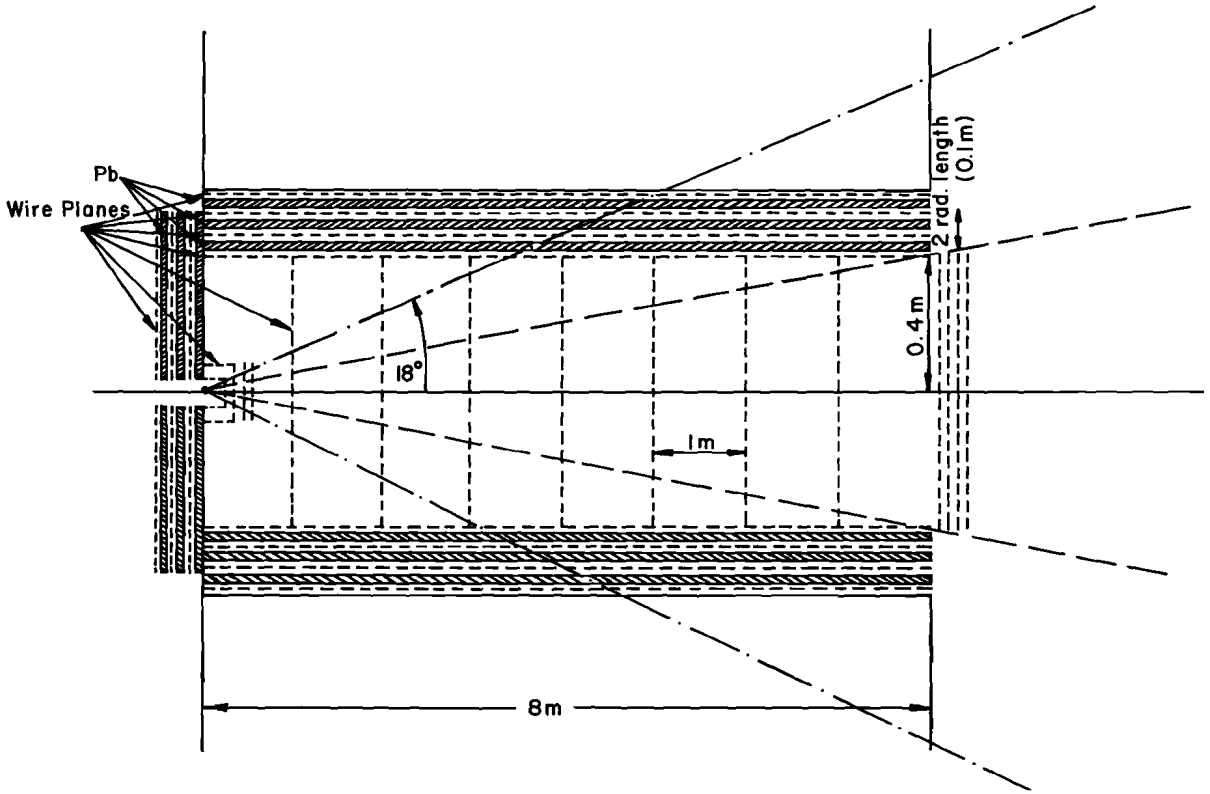

Fig. 7. Vertical section of the magnet and counter system to study the reaction $\pi p \rightarrow pX \rightarrow p\pi p \rightarrow p3\pi$ at 100 GeV/c. The downstream planes, 16 in. from the magnet exit are not shown. See text for full description.

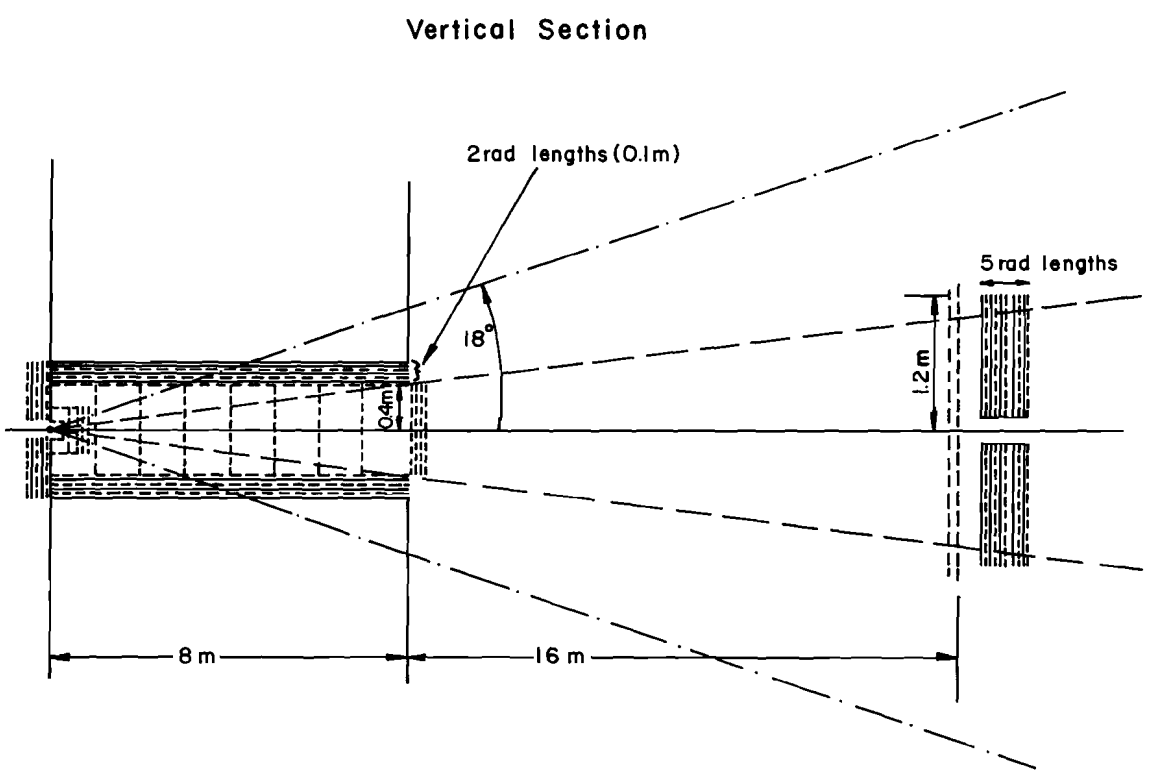

Fig. 8. As Fig. 7, with the downstream lever arm included.

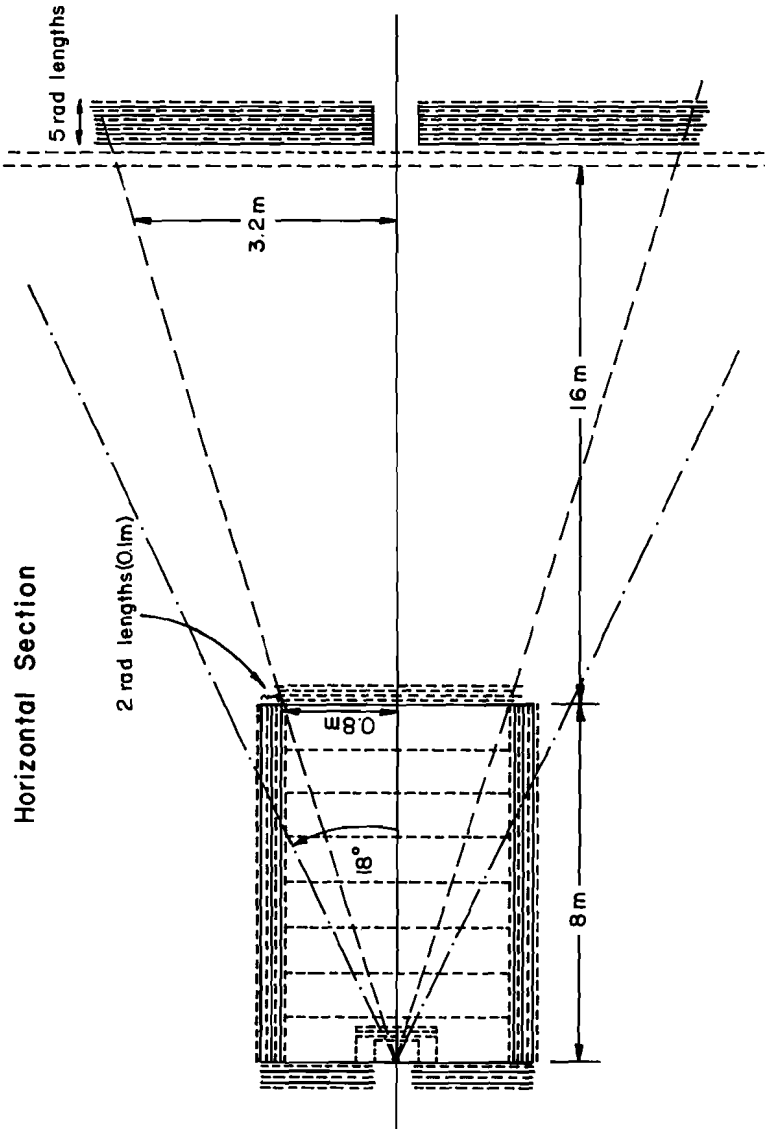

Fig. 9. As Fig. 8, horizontal section.

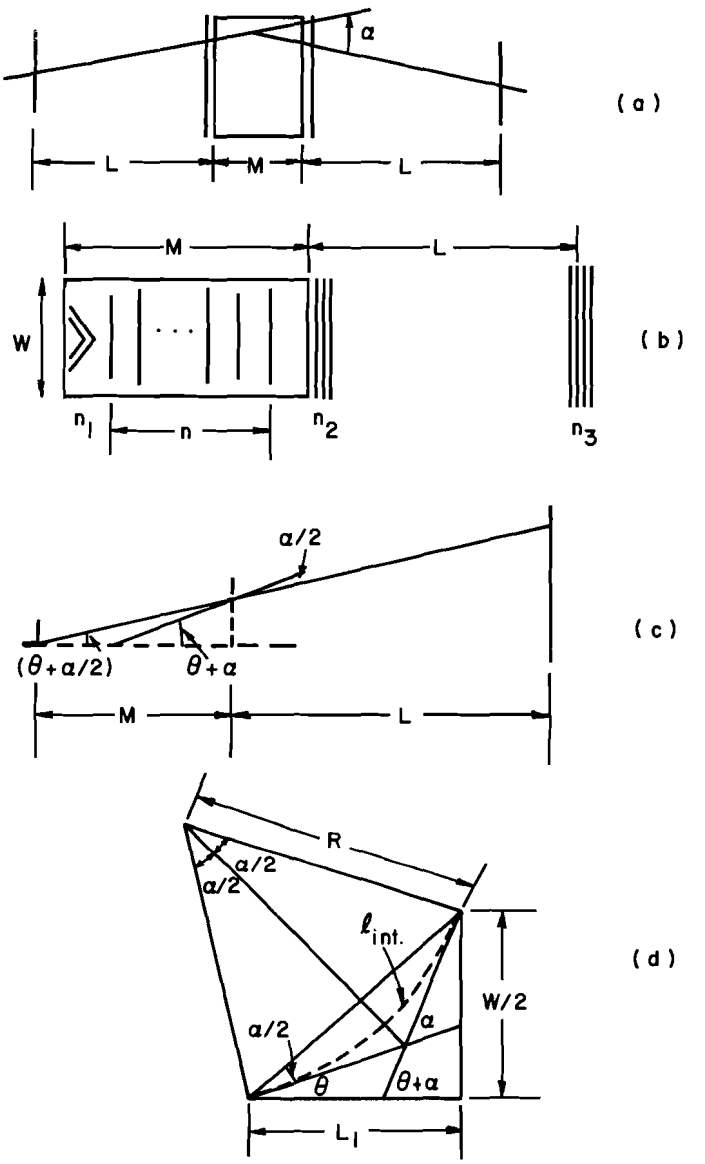

Fig. 10. Diagrams of various magnet and lever arm systems, defining quantities used in Appendix I. See text for a full description.

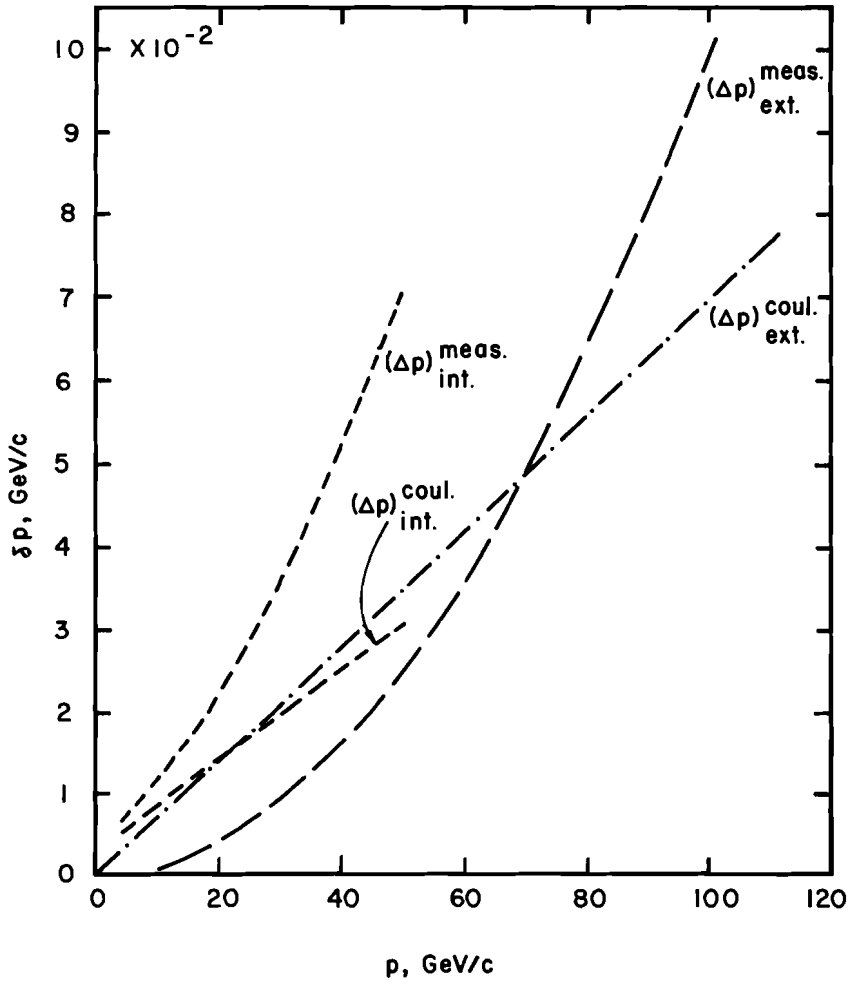

Fig. 11. Errors in pion momenta measured using magnetic spectrometer drawn in Figs. 6 to 9.

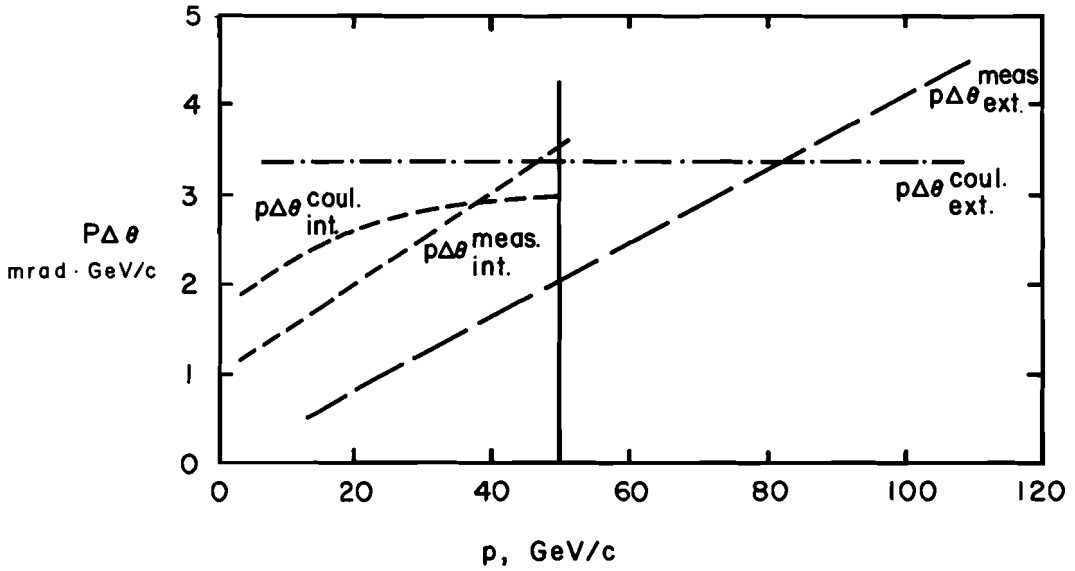

Fig. 12. Errors in measuring transverse momenta of pions measured using magnetic spectrometer of Figs 6 to 9.

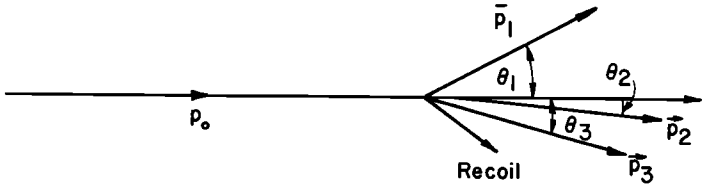

Fig. 13. Quantities used in Appendix II.

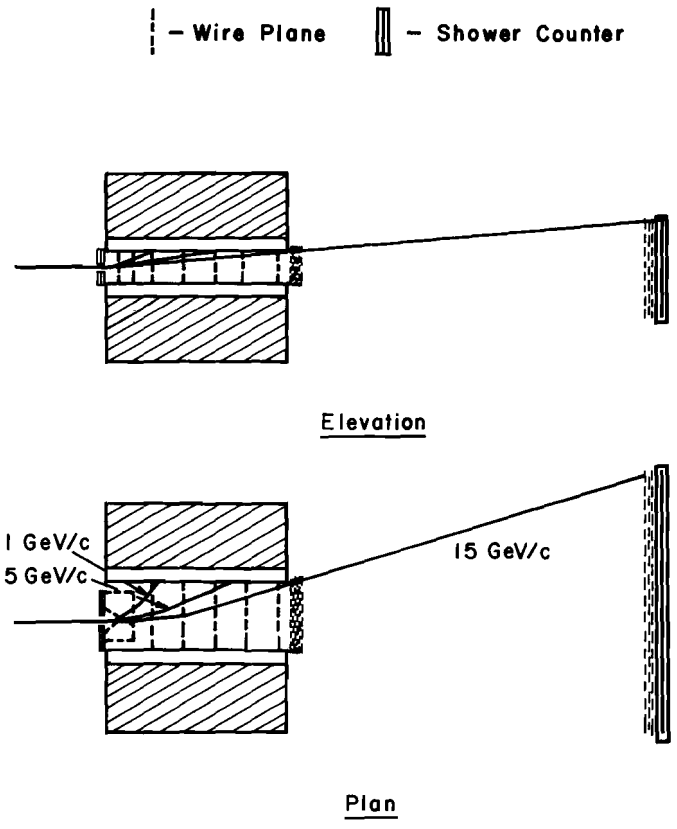

Fig. 14. Alternative design of magnetic spectrometer to study the reaction $\pi p \to pX \to p3\pi$ at 100 GeV/c. See Appendix II for details.

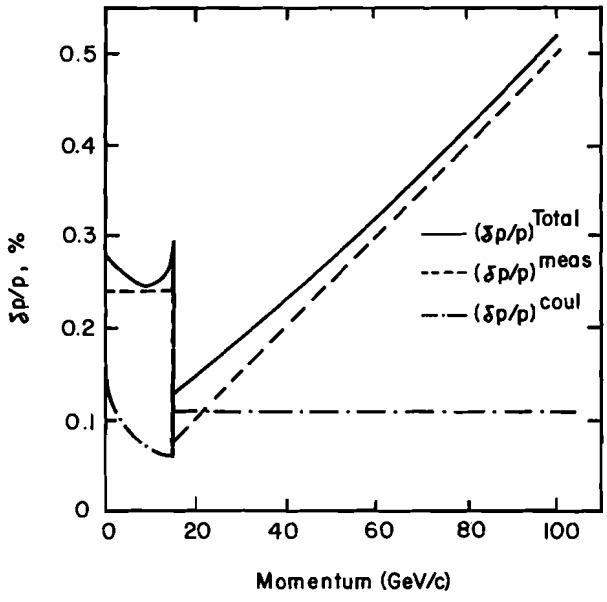

Fig. 15. Errors in pion momenta measured in the spectrometer of Fig. 14.

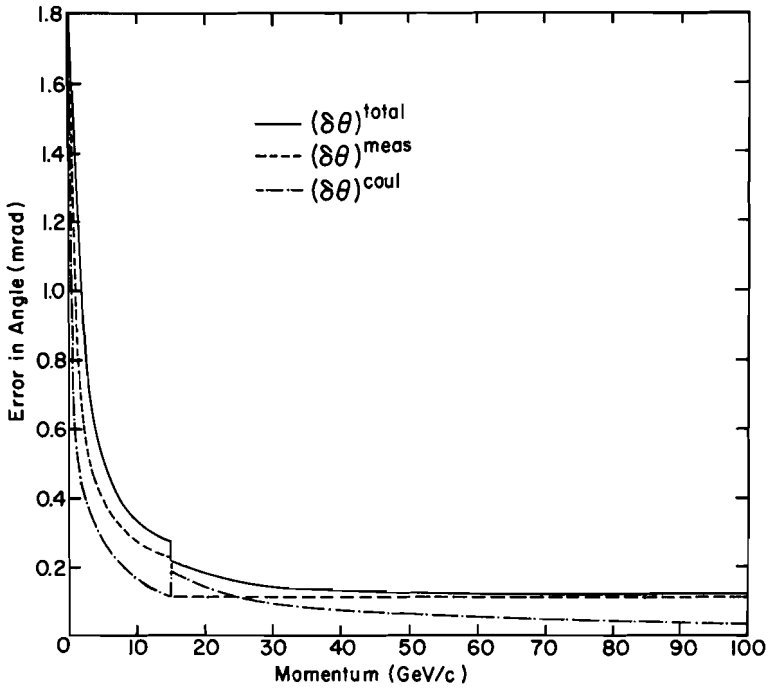

Fig. 16. Errors in angle of pions measured in the spectrometer of Fig. 14.